Journal of
Mechanics of
Materials and Structures

STUDIES ON PERFORMANCE AND FAILURE MODE OF T-SHAPED DIAPHRAGM-THROUGH CONNECTION UNDER MONOTONIC AND CYCLIC LOADING

Bin Rong, Changxi Feng, Ruoyu Zhang, Shuai Liu and Guangchao You

Volume 13, No. 1 January 2018

msp

JOURNAL OF MECHANICS OF MATERIALS AND STRUCTURES
Vol. 13, No. 1, 2018
dx.doi.org/10.2140/jomms.2018.13.1

STUDIES ON PERFORMANCE AND FAILURE MODE OF T-SHAPED DIAPHRAGM-THROUGH CONNECTION UNDER MONOTONIC AND CYCLIC LOADING

BIN RONG, CHANGXI FENG, RUOYU ZHANG, SHUAI LIU AND GUANGCHAO YOU

This paper examines the mechanical properties of T-shaped diaphragm-through connections between CFST columns and steel beams under monotonic and cyclic loading. A monotonic test and a cyclic test on two same specimens are described. The experimental setup, connection configurations, and material properties are firstly introduced, followed by a detailed account of the results and observations from tests. The failure mode and the ultimate bearing capacity are similar in the two tests, while the connection exhibits larger yield capacity and lower ductility under cyclic loading than monotonic loading. Nonlinear finite element analysis was also employed in this investigation. The predicted results are in good agreement with the experimental ones so that the reliability of finite element analysis is verified. Diaphragm-through connection and ordinary beam-column connection are simulated and compared through FEM, and failure modes of plastic hinge at beam end and column face yielding are found respectively, which indicates a significant strengthening effect of the diaphragm and the superior mechanical properties of the diaphragm-through connection.

1. Introduction

As the hinge of force transferring, beam-column connections are the main components that transmit loads in the whole structure. Diaphragm-through connection between concrete-filled square tubular (CFST) columns and steel beams has gained a widespread usage in composite frame structures because of its good bearing capacity, ductility, seismic-resisting, and constructional convenience.

As a typical rigid beam-column connection, there are a large number of researches conducted on the diaphragm-through connection. Experimental studies on connections comprising high-strength steel and concrete were carried out by Nishiyama et al. [2004] and Fukumoto and Morita [2005] and new computing models and calculating methods of shear capacity were proposed, and the calculated results agree well with the experimental results. Finite element analyses were conducted under both monotonic loading and cyclic loading by Nie et al. [2008] and were compared with a series of cyclic loading experiments of fourteen cruciform connection specimens to analyze the mechanical behavior of these three types of connection. Rong et al. [2012] used the finite element method to analyze the tensile behavior and seismic behavior of the panel zone of diaphragm-through connections. The numerical data had a good agreement with the test results. Qin et al. [2014b] tested four full-scale specimens of existing and proposed through-diaphragm connections to concrete-filled rectangular steel tubular columns subjected to cyclic loading. The variables taken into consideration in the experiments include the geometry of the

Keywords: diaphragm-through connection, monotonic and cyclic tests, mechanical property, finite element analysis, ordinary beam-column connection, failure mode, strengthening effect of diaphragm.

through-diaphragm, the configuration of the weld access hole, horizontal stiffeners, and the methods of connecting beam webs to columns. Qin et al. [2014a] carried out theoretical studies into the behavior of the through-diaphragm to concrete-filled rectangular hollow section columns subjected to tensile force. In that study, component-based mechanical models were proposed to predict the strength of the column component of concrete-filled rectangular hollow section columns under tensile load imparted through a through-diaphragm connection, and the mechanical models were compared with a large range of experimental results and good agreement was shown between them. Based on finite element models of the internal diaphragm connection and through-diaphragm connection set up by [Yu et al. 2015], the out-of-plane deformation at the column flange, force flow pattern, and shear and moment transfer efficiency of a WF-beam to rectangular CFT column connection were discussed, and the results show that both the Poisson effect and flexibility of column flange leads to a change on the force flow pattern in the beam-column junction region and inefficient moment transferring ability through the beam web, resulting in a high level of hydrostatic stress demand at the beam flanges. Rong et al. [2016] tested four specimens under static tension loads and adapted the finite element method to study the mechanical properties and bearing capacity of diaphragm-through joints with a failure mode of panel zone; computational models of yield lines on a square steel tube and diaphragm were established based on the distribution pattern of the plastic zone, and an analytical method for the evaluation of the bearing capacity of the joint was proposed.

At present the experimental studies on diaphragm-through connection can be classified as two types: flexural capacity studies and shear capacity studies. The former refers to some researches on the flexural capacity of diaphragm-through connection based on static tension tests, while the latter refers to those hysteretic tests carried out to study the shear capacity and seismic behavior of the diaphragm-through connection. Most studies on diaphragm-through connection belong to the two types, while the study on the comparison of performance of diaphragm-through connection under monotonic and cyclic loading is little. Therefore, there is a need for further assessment and characterization of the performance of the diaphragm-through connection under monotonic and cyclic loading conditions.

This paper examines the experimental responses of two T-shaped diaphragm-through connections under monotonic and cyclic loading respectively, where T-shaped connections mean exterior connections of a frame structure. It presents and discusses the results of monotonic and cyclic tests. A detailed description of the testing arrangement and material properties is given, and the main experimental results and salient behavioral observations are discussed. The discussion focuses on the comparisons of issues related to stiffness, capacity and failure mechanisms between monotonic and cyclic tests. In addition, the relationship of failure mode and the ratio of beam width and column width is analyzed in this paper. Finally, nonlinear finite element models are also developed and validated against experimental results in this investigation. Using finite element analysis, diaphragm-through connection and ordinary beam-column connection are simulated and compared, and different failure modes of the two kinds of connection and the causes of the failure modes are studied particularly.

2. Experimental program

2.1. ***Test specimens.*** In order to investigate the behavior of a T-shaped diaphragm-through connection under monotonic and cyclic loading, two specimens named SJ1 and SJ2 with same size were designed to carry out a monotonic test and a cyclic test respectively. The specimen details are shown in Figure 1. As

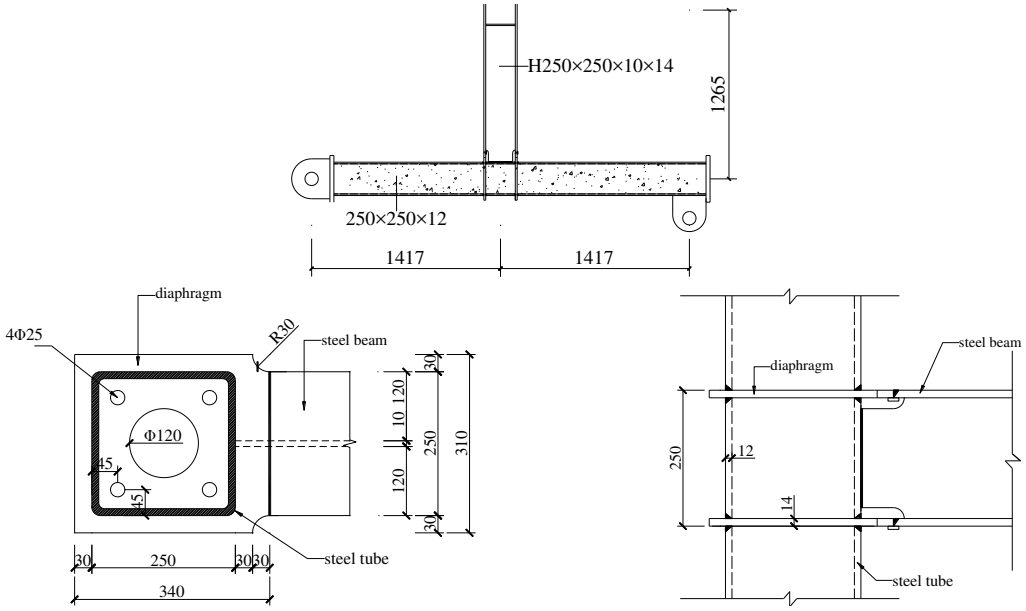

Figure 1. Details of the T-shaped diaphragm-through connection: T-shaped specimen (top), overhead view (left), and section view (right).

thickness (mm)	f_y (N/mm^2)	f_u (N/mm^2)	E_s (105 N/mm^2)
10	272.6	352.7	2.04
12	313.7	439.8	2.01
14	252.2	414.6	2.03

Table 1. Material properties of concrete.

grade	f_c (N/mm^2)	E_c(10^4 N/mm^2)
C30	38.4	3.49

Table 2. Material properties of steel.

seen in the figure, the distance between the panel zone and two hinges is equal so that the force situation of the two side columns is symmetric. The steel tubes were manufactured from cold-formed square steel tubes, and the diaphragms and beams were welded by steel plates. The C30 concrete in columns was cured for 28 days.

A material test was carried out, in which tension coupons were cut from steel tubes and steel plates and were tested to determine the material properties of the steel. The yield strength f_y, the ultimate strength f_u, and the modulus of elasticity E_s, are listed in Table 1. Concrete cubes were cast and cured in the conditions same to those of the experiments and tested under pressure load. The measured average axial compressive strength f_c and the module of elasticity E_c are listed in Table 2.

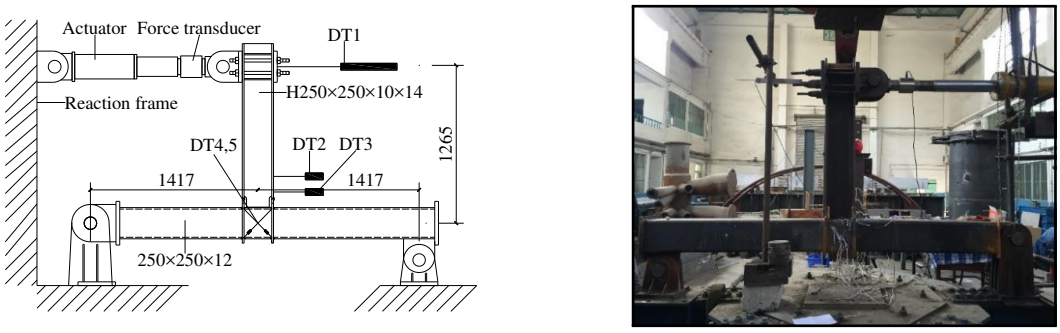

Figure 2. Test setup: schematic drawing and photo.

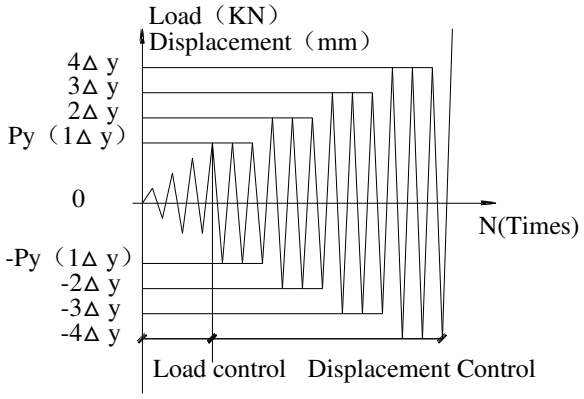

Figure 3. Regulation of cyclic loading system.

2.2. ***Experimental arrangement and loading procedure.*** The arrangement used for testing T-shaped diaphragm-through connections is shown in Figure 2. The specimens were placed horizontal on the testing frame and a 1000 kN level hydraulic actuator whose displacement range was ±350 mm operating in load and displacement control was used to apply horizontal deformation at the free beam end. The tubular column was restrained at both ends with the aid of a hinged support and a slotted hole hinge support. DT1 (displacement transducer) was used to measure the control displacement at the free beam end corresponding to the location of horizontal actuator, while the local deformation of the restrained beam end was measured by DT2 and DT3. The diagonal displacement of the shear panel was measured by DT4 and DT5, as shown in Figure 2 (left). The mechanical testing and simulation (MTS) data collecting system was used to collect the measured data automatically.

Load-displacement hybrid control was used to control the horizontal cyclic load applied on the free beam end. Before testing, every specimen was preloaded twice to check the reaction of the test arrangement and the measuring devices. For the cyclic test, stepwise force load was applied to the beam end and recycled one time at each step loading before yield. After yield, the load would be controlled by multiplying the yield displacement Δ_y (horizontal displacement of the beam end when specimens yield), and recycled three times for each step, as shown in Figure 3 [Kataoka and El Debs 2015; Yin et al. 2016].

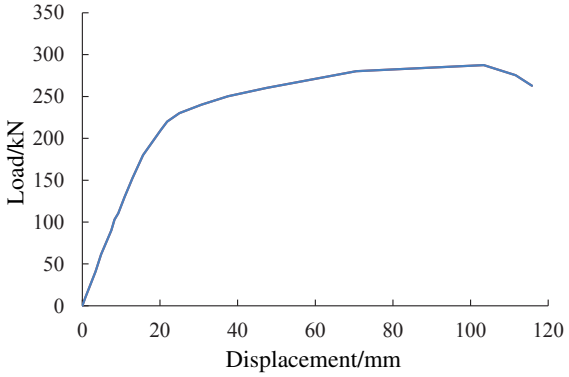

Figure 4. Load-displacement curve of SJ1.

For the monotonic test, the load system was the same as the cyclic test, except that the specimen was pushed along one direction without recycle until failure.

3. Experimental results and observations

The corresponding deformation patterns and load-displacement relationships are presented in Figures 4–7, and the main response parameters obtained from the tests are summarized in Table 3, such as the yield load p_y^e and the failure load p_u^e. A graphical method [Park et al. 2010] is employed to catch the initial stiffness and the yield load p_y^e at global connection yield. The ductility factor μ is defined as $\mu = \Delta_u/\Delta_y$, where Δ_y and Δ_u mean the yield displacement and the ultimate displacement obtained from load-displacement curve of monotonic test and skeleton curve of cyclic test respectively. In this section, the main behavioral patterns are discussed and the salient response characteristics such as stiffness, strength, and ductility factor are examined [Tizani et al. 2013]. Particular focus is given in the discussion comparing monotonic behavior and hysteretic response under cyclic loading [Elghazouli et al. 2009; Málaga-Chuquitaype and Elghazouli 2010]. In addition, the influence of the ratio of beam flange width to column flange width on failure modes of connection is discussed.

3.1. ***Monotonic test.*** SJ1 was tested under monotonic load until failure. The load-displacement curve is shown in Figure 4. It is found that SJ1 behaved in a relatively ductile manner. The curve exhibits elastic behavior at the initial stage followed by a clear extensive plastic plateau indicating good ductility. At a load of 243.1 kN corresponding to 20.6 mm displacement, the restrained end of the beam yielded but no obvious phenomenon was observed. Beyond this point, load was continued monotonously with displacement controlled by applying equal multiples of yield displacement on the free beam end. As the load increased, the compression flange of the restrained beam end started to buckle, as shown in Figure 5. The load reached its peak value of 287.5 kN corresponding to 103.4 mm displacement. Finally, the specimen failed with a plastic hinge appearing at the restrained beam end. The specimen was then unloaded and the test was terminated.

3.2. ***Cyclic test.*** In contrast to SJ1, SJ2 was loaded cyclically until failure and its failure mode was similar to that of SJ1. Figures 6 (left and right) are the hysteretic curve and the skeleton curve of SJ2 respectively. At a load of 267.5 kN corresponding to 24.1 mm displacement, there was no obvious yield

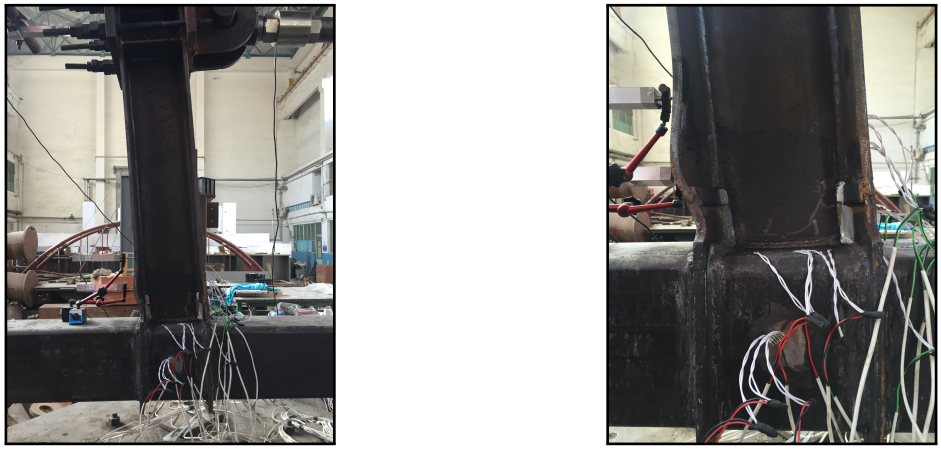

Figure 5. Behavior of SJ1.

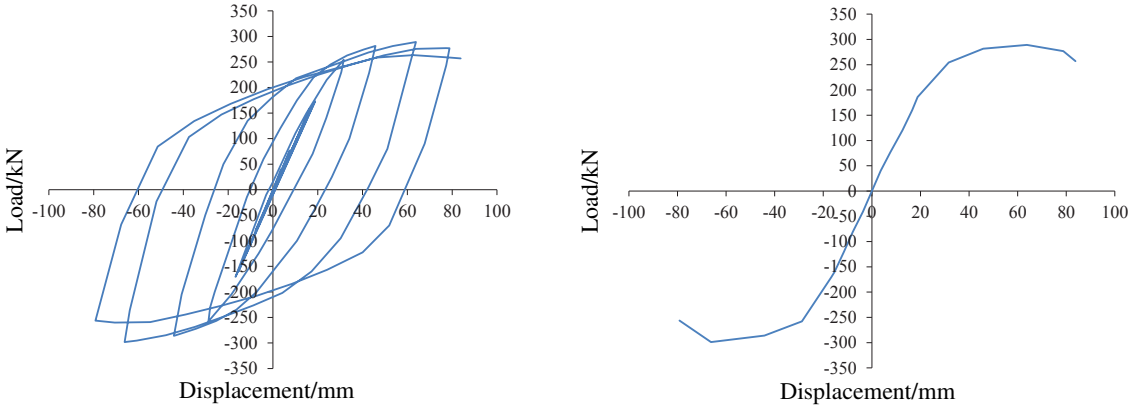

Figure 6. Load-displacement curve of SJ2: hysteretic curve (left) and skeleton curve (right).

Figure 7. Behavior of SJ2.

specimen	initial stiffness (kN/m)	Δ_y (mm)	p_y^e (kN)	Δ_u (mm)	p_u^e (kN)	μ
SJ1	11.8	20.6	243.1	103.4	287.5	5.5
SJ2	11.1	24.1	267.5	63.8	289	2.6

Table 3. Summary of results.

deformation, but an inflection point was observed in the load-displacement curve. Beyond this point, load was continued cyclically with displacement controlled by applying equal multiples of yield displacement on the free end. As the load was increasing, the local buckling initiated in the flange of the restrained beam end. The peak load of SJ2 was 289 kN corresponding to 63.8 mm displacement. Finally, the plastic hinges appeared at the restrained beam end and the capacity dropped to 84% of the peak load when it was subjected to five times the yield displacement, which means the failure of SJ2. Then the specimen was unloaded and the test was terminated.

3.3. *Discussion.*

3.3.1. *Comparison of monotonic behavior and hysteretic response.* As shown in Figures 5 and 7, failure modes of SJ1 and SJ2 are both plastic hinge damage, and the failure load p_u^e of SJ1 and SJ2 are nearly equal, which indicates that different loading types, static load and seismic action, have little effect on the ultimate bearing capacity of a T-shaped diaphragm-through connection. The initial stiffness of SJ1 is approximate to SJ2, but SJ2 yielded at a larger displacement, so that the yield load p_y^e of SJ2 is a little larger than that of SJ1. In consideration of ductility factor μ illustrated in Table 3, T-shaped diaphragm-through connection under monotonic loading has better ductility than cyclic loading. In addition, SJ2 failed at a lower displacement for that cyclic test consumed more energy.

3.4. ***Ratio of beam flange width to column flange width.*** Research by [Lu 1997] showed that the ratio of beam flange width to column flange width β has great influence on the failure mechanism of a multiplanar tubular joint. It was thought that the failure mode of the connection is the punching shear failure at the column flange when β is approximately 1. According the tests described before, the ratio of beam flange width to column flange width of specimens is equal to 1, while the failure modes of SJ1 and SJ2 are not column flange damage but plastic hinge damage at the beam end, which indicates that the theory is not suitable for a diaphragm-through connection. The applicability of this theory will be discussed specifically in finite element analysis. Therefore, the limitation on the ratio of beam flange width to column flange width of a T-shaped diaphragm-through connection can be extended to 1 so that it can make full use of the bearing capacity of beam under the premise of beam damage prior to column damage.

4. Finite element analysis

In order to investigate the influences of the presence of diaphragm and the ratio of beam flange width to column flange width on failure modes of beam-column connections, a parametric finite element analysis has been undertaken using the finite element package ANSYS [Lee et al. 2012; Yu et al. 2015]. The three-dimensional finite element model DT1 in finite element analysis, designed to verify the feasibility of finite element analysis, has the same sizes and material properties as the specimens in monotonic and cyclic tests described before. Then in this study, factors that were taken into discussion include:

model	column size	beam size	β	presence of diaphragm
DT1	250×12	$250\times250\times10\times14$	1	diaphragm-through
DT2		$250\times225\times10\times14$	0.9	diaphragm-through
DT3		$250\times175\times10\times14$	0.7	diaphragm-through
WD1		$250\times250\times10\times14$	1	without diaphragm
WD2		$250\times225\times10\times14$	0.9	without diaphragm
WD3		$250\times175\times10\times14$	0.7	without diaphragm

Table 4. List of models.

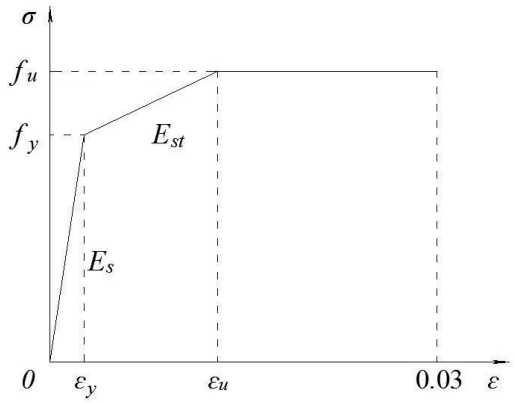

Figure 8. Constitutive law of steel members.

the presence of diaphragm and the ratio of beam flange width to column flange width. Key factors of different models are marked in Table 4. DT series are the models of diaphragm-through connections while WD series are beam-column connections without diaphragm. Two comparison series are the same in column and beam dimensions.

4.1. *Finite element model.*

4.1.1. *Steel members modeling.* The three-dimensional 20-node element SOLID 186 is adopted to model the steel tube, the diaphragm, the beam flange, and the beam web. Each node of the element has three translation degrees of freedom. This element is capable of capturing plasticity, large deflections, and large strains.

As shown in Figure 8, the trilinear stress-strain relation proposed by Nie et al. [2008] is used to model the constitutive law of the steel members, where $\varepsilon_y = f_y/E_s$ and $\varepsilon_u = 10(f_u - f_y)/E_s$. The values of the yield strength f_y, the ultimate strength f_u, and the modulus of elasticity E_s are the values found in the material test. The Poisson's ratio of the steel members is assumed as 0.3.

4.1.2. *Concrete modeling.* The three-dimensional 8-node element SOLID 65 is used to model the infilled concrete. Each node of the element has three translation degrees of freedom. This element is capable of capturing the effects of cracking in tension, crushing in compression, and plastic deformation.

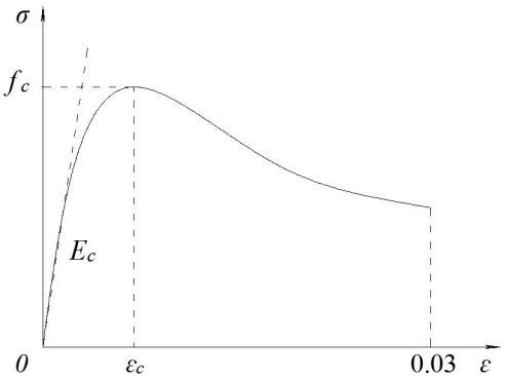

Figure 9. Constitutive law of concrete.

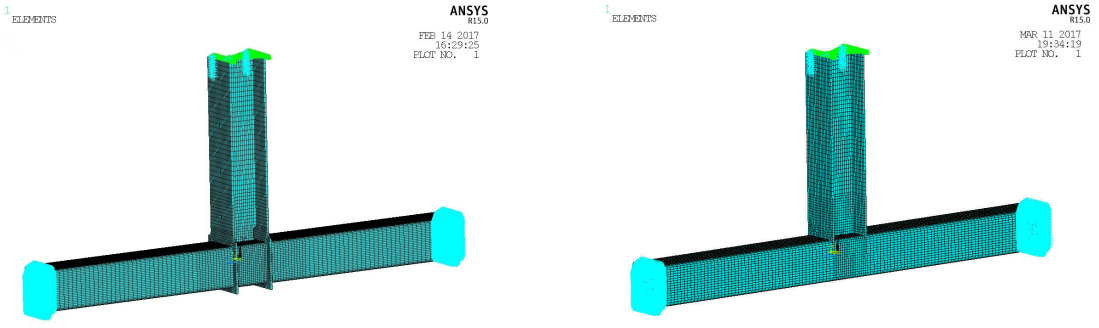

Figure 10. Finite element model: DT series (left) and WD series (right).

The constitutive law of concrete used for the infilled concrete is shown in Figure 9 [Li and Han 2012]. The values of the compressive strength σ_c and the modulus of elasticity E_c of the concrete are the values found in the material test. The Poisson's ratio of the infilled concrete is assumed equal to 0.2.

4.1.3. *Modeling of the concrete-steel interface.* The contact elements TARGE 170 and CONTA 174 are employed to model the contact action between the steel members and the concrete. These contact elements allow the surfaces to separate but not penetrate each other. They combine as a contact pair through sharing a real constant. The coefficient of friction between the two faces is taken as 0.25 in the analysis.

4.1.4. *Modeling of loading and boundary conditions.* The same loading procedures and constraints as the experiments should be used in the finite element analysis. To simulate this action, the columns were held horizontally, the top and the bottom of column were fixed and the loads were applied on the free beam end. The loads were applied as static uniform load using displacement control at each node of the loaded surfaces, and the displacement increments are identical to the increments of the monotonic test and the cyclic test. The finite element models are shown in Figure 10.

4.2. ***Numerical results.*** Among all models, the reference model DT1 was subjected to monotonic loading and cyclic loading (as the tests described before) while the others were only subjected to monotonic loading. The failure models and load-displacement relationships of DT1 and test specimens are compared

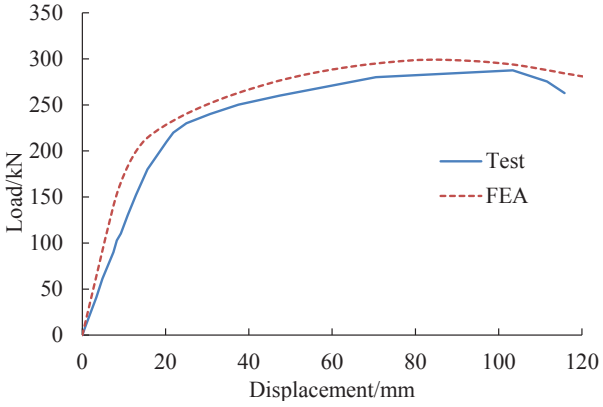

Figure 11. Comparison of load-displacement curve for SJ1.

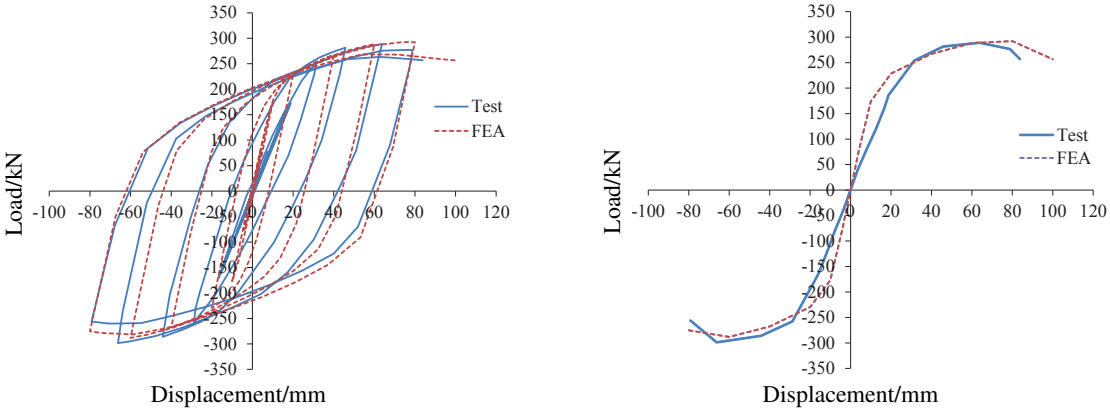

Figure 12. Comparison of load-displacement curve for SJ2: hysteretic curve (left) and skeleton curve (right).

to verify the feasibility and accuracy of the finite element analysis. The influences of the presence of diaphragm and the ratio of beam flange width to column flange width on failure modes of beam-column connections are studied using experimental results and finite element analysis.

4.2.1. *Model verification.* In order to verify the accuracy of the finite element models, load-displacement curves obtained from the finite element model DT1 are compared with test curves in Figures 11 and 12, and it is found that all load-displacement curves match with the experimental ones well. The yield load p_y^e and the failure load p_u^e of numerical results obtained from the predicted curves by using the graphical method [Park et al. 2010] are listed in Table 5 and they are compared with the experimental ones. The analytical values are in good agreement with the experimental ones. The overall agreement between the experimental and the numerical results demonstrates the feasibility and accuracy of the finite element analysis, therefore it is reasonable to study the influences of the presence of diaphragm and the ratio of beam flange width to column flange width on failure modes of beam-column connections [Liu et al. 2012; 2014].

specimen	yield bearing capacity			ultimate bearing capacity		
	p_y^e (kN)	p_y^f (kN)	p_y^f/p_y^e	p_u^e (kN)	p_u^f (kN)	p_u^f/p_u^e
SJ1	243.1	259.9	1.069	287.5	299.1	1.040
SJ2	267.5	255.7	0.956	289	292.3	1.011

Table 5. Comparison of bearing capacity.

4.2.2. *Failure modes and load-displacement curves.* Typical predicted failure modes and stress contours of DT series and WD series are shown in Figure 13. The predicted failure modes of the two series are obviously different. As shown in Figure 13 (left column), the failure mode of DT series is plastic hinge damage at the beam end and it is caused by overstress of the beam end near the panel zone of the connection. The right column shows that the failure mode of WD series is column face yielding, and there is apparently large local deformation on the column flange face, which means the failure of WD series is caused by the over-deformation of the column face. Therefore, WD series are supposed to be defined as failure when local deformation of column face reaches 3% of the beam width, even though the load still increases steadily.

The load-displacement curves obtained by the finite element analysis are compared with each other in Figure 14. The predicted load-displacement curves of all models have a linear elastic behavior at the initial stage followed by inelastic behavior when the load is further increased. The curves show that the initial stiffness and the bearing capacity of DT series are obviously larger than WD series, for the diaphragm strengthens the DT series, which results in the superior mechanical properties of the diaphragm-through connection. For DT series, the failure model is plastic hinge damage at the beam end, therefore it is reasonable that the bearing capacity decreases as beam width get smaller. However, there is also a negative correlation between the bearing capacity and beam width for WD series when its failure mode is column face yielding. As illustrated in Figure 15, different beam widths cause different yield lines on the column face, and larger beam width means a larger yield region of the column face, which results in larger bearing capacity.

4.3. ***Discussion on failure mode of beam-column connection.*** According to research on beam-column connection carried out by Lu [1997] described before, the ratio of beam flange width to column flange width β greatly influences the failure mechanism of a multiplanar tubular joint. There are three kinds of failure mechanism for a column classified by β: column face yielding ($\beta \leq 0.85$), punching shear failure ($0.85 \leq \beta < 1 - 1/\gamma$), and flange failure ($\beta = 1$), where γ is the width to thickness ratio of the column. In combination with the theory, this section discusses influences of diaphragm and β of failure modes of beam-column connections through finite element analysis.

WD series are designed to verify the accuracy of the theory. Since cracks were not considered in numerical analyses and infilled concrete prevented the failure of the column flange, only column face yielding could be modeled by FEM. As shown in Figure 13, the failure modes of WD series are all column face yielding, which agrees well with the theory of Lu [1997] and verifies its accuracy for ordinary beam-column connections without diaphragm.

DT series are models of diaphragm-through connection, and there is no difference between DT series and WD series except for the presence of a diaphragm. However, failure modes of the two series are

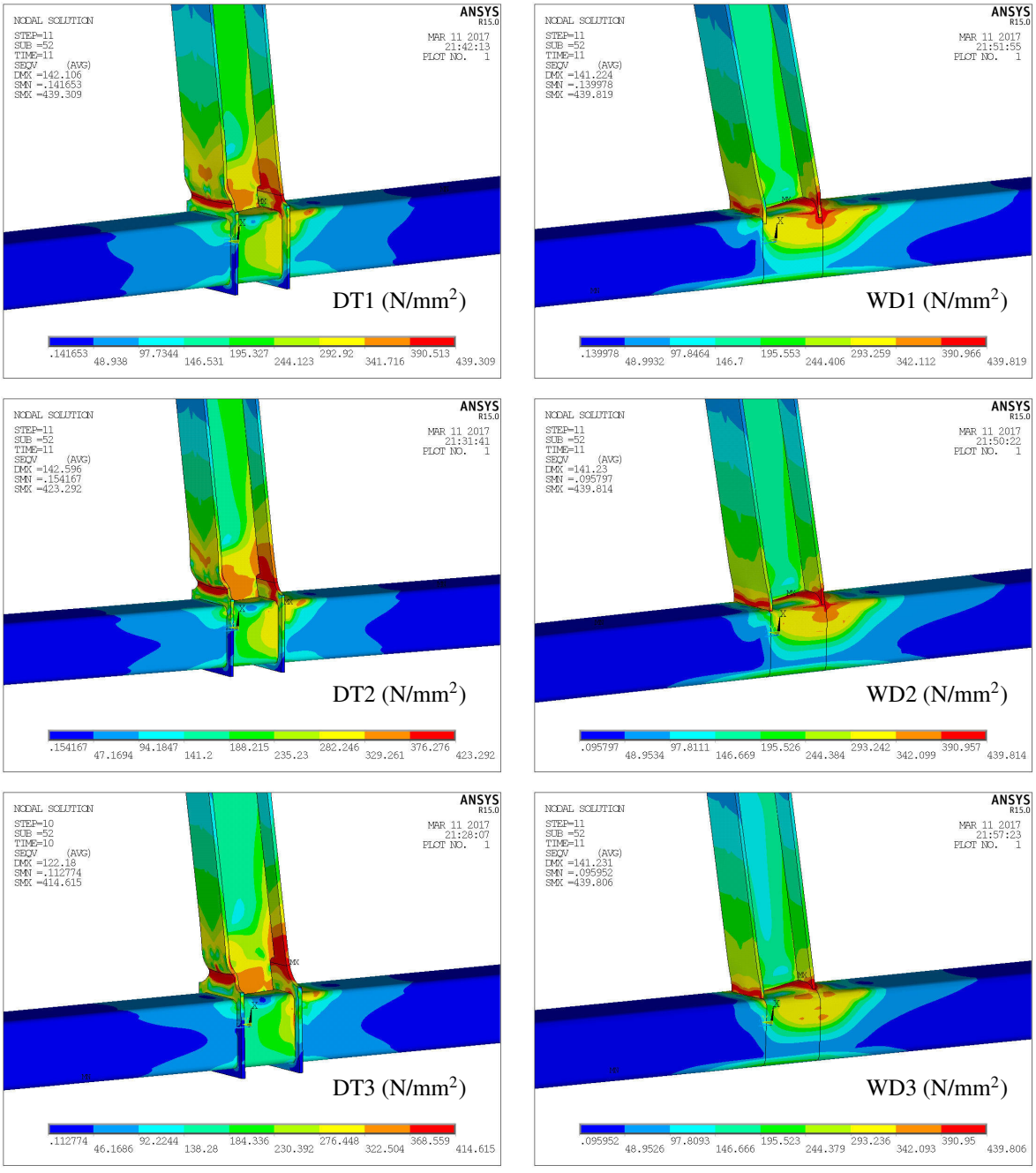

Figure 13. Failure modes and von Mises stress contour of models.

totally different. According to the theory of Lu [1997], the failure modes of DT series are also supposed to be column failure. However, failure modes of DT series are all plastic hinge at the beam end, which disagrees with the theory. Therefore, the theory of Lu [1997] is not suitable for diaphragm-through

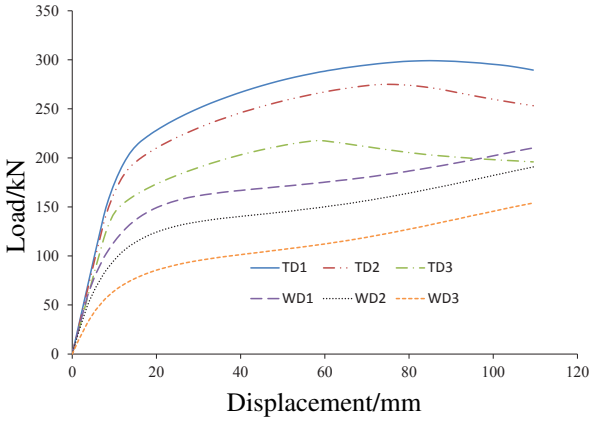

Figure 14. Load-displacement curves of models.

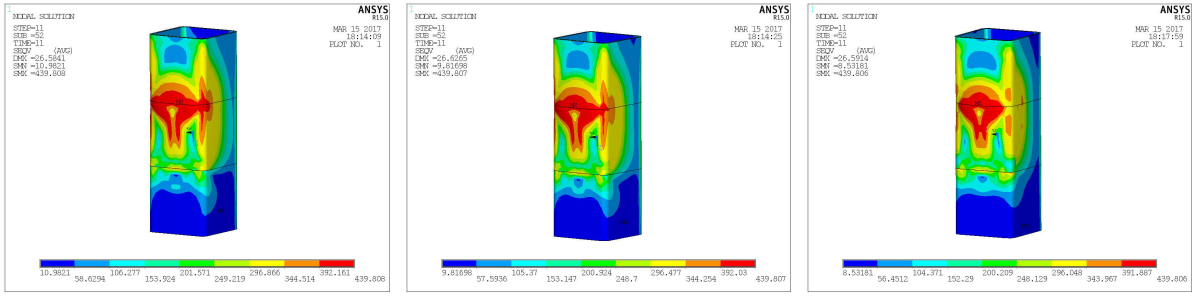

Figure 15. Column face yielding of WD series (from left to right): WD1, WD2, and WD3.

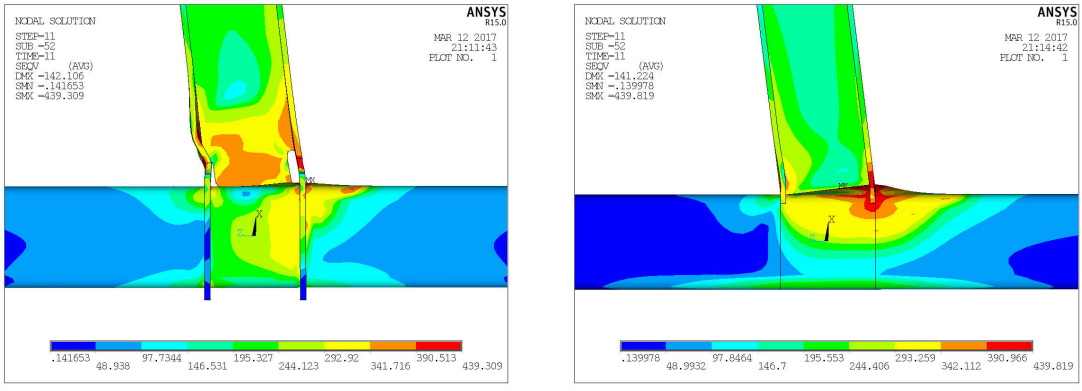

Figure 16. Failure modes of DT1 (left) and WD1 (right).

connections. Figure 16 illustrates the failure modes of DT1 and WD1 clearly; it is found that the stress level distribution for them are obviously different. For DT1, the high stress level regions of DT1 focus on the junction part of the beam and diaphragm while the stress level of the column is much lower. However, as the distribution of WD1 is revised, high stress level on the column but low stress level on the beam appear in WD1. The phenomenon demonstrates the great influence of the diaphragm on the failure mode

of beam-column connection. The diaphragm strengthens the column greatly, and it results in the turn of failure mode from column face yielding to plastic hinge damage at the beam end.

5. Conclusions

In this paper, tests and finite element analysis were undertaken to investigate mechanical properties of T-shaped diaphragm-through connections between CFST column and steel beam under monotonic and cyclic loading. The main conclusions can be drawn as follows:

- Experimental results show that the failure modes of the two specimens are both plastic hinge damage at the restrained beam end. Different loading types, static load and seismic action, have little effect on the failure mode and ultimate bearing capacity of the T-shaped diaphragm-through connection, and the connection exhibits larger yield capacity and lower ductility under cyclic loading than monotonic loading. In addition, it is also found that the failure mode of a T-shaped diaphragm-through connection whose ratio of beam flange width to column flange width is 1 is plastic hinge damage at beam end.
- According to parametric finite element analysis, which is in a good agreement with the test results, the initial stiffness and the bearing capacity of diaphragm-through connection are obviously larger than ordinary beam-column connection, and there is also a negative correlation between the bearing capacity and beam width for both the diaphragm-through connection and ordinary beam-column connection.
- The failure mode of the T-shaped diaphragm-through connection is plastic hinge damage, which is caused by overstress of the restrained beam end. However, the failure mode of the beam-column connection without diaphragm is column face yielding, which is caused by a large local deformation on the column flange face. The phenomenon demonstrates that the diaphragm strengthens the column greatly, and it results in the turn of the failure mode from column face yielding to plastic hinge damage at beam end.

Acknowledgements

The research described in this paper was financially supported by the National Natural Science Foundations of China (No. 51268054 and No. 51468061) and the Natural Science Foundation of Tianjin City, China (No. 13JCQNJC07300). The financial supports are greatly appreciated.

References

[Elghazouli et al. 2009] A. Y. Elghazouli, C. Málaga-Chuquitaype, J. M. Castro, and A. H. Orton, "Experimental monotonic and cyclic behavior of blind-bolted angle connections", *Eng. Struct.* **31**:11 (2009), 2540–2553.

[Fukumoto and Morita 2005] T. Fukumoto and K. Morita, "Elastoplastic behavior of panel zone in steel beam-to-concrete filled steel tube column moment connections", *J. Struct. Eng.* **131**:12 (2005), 1841–1853.

[Kataoka and El Debs 2015] M. N. Kataoka and A. L. H. d. C. El Debs, "Beam-column composite connections under cyclic loading: an experimental study", *Mater. Struct.* **48**:4 (2015), 929–946.

[Lee et al. 2012] S. H. Lee, Y. H. Kim, and S. M. Choi, "Shear strength formula of CFST column-beam pinned connections", *Steel Compos. Struct.* **13**:5 (2012), 409–421.

[Li and Han 2012] W. Li and L.-H. Han, "Seismic performance of CFST column to steel beam joint with RC slab: joint model", *J. Constr. Steel Res.* **73** (2012), 66–79.

[Liu et al. 2012] Y. Liu, C. Málaga-Chuquitaype, and A. Y. Elghazouli, "Response and component characterisation of semi-rigid connections to tubular columns under axial loads", *Eng. Struct.* **41** (2012), 510–532.

[Liu et al. 2014] Y. Liu, C. Málaga-Chuquitaype, and A. Y. Elghazouli, "Behaviour of open beam-to-tubular column angle connections under combined loading conditions", *Steel Compos. Struct.* **16**:2 (2014), 157–185.

[Lu 1997] L. H. Lu, *The static strength of I-beam to rectangular hollow section column connections*, Ph.D. thesis, Delft University of Technology, 1997, available at http://tinyurl.com/staticlu.

[Málaga-Chuquitaype and Elghazouli 2010] C. Málaga-Chuquitaype and A. Y. Elghazouli, "Behavior of combined channel/angle connections to tubular columns under monotonic and cyclic loading", *Eng. Struct.* **32**:6 (2010), 1600–1616.

[Nie et al. 2008] J. Nie, K. Qin, and C. S. Cai, "Seismic behavior of connections composed of CFSSTCs and steel-concrete composite beams: finite element analysis", *J. Constr. Steel Res.* **64**:6 (2008), 680–688.

[Nishiyama et al. 2004] I. Nishiyama, T. Fujimoto, T. Fukumoto, and K. Yoshioka, "Inelastic force-deformation response of joint shear panels in beam-column moment connections to concrete-filled tubes", *J. Struct. Eng.* **130**:2 (2004), 244–252.

[Park et al. 2010] S.-H. Park, S.-M. Choi, Y.-S. Kim, Y.-W. Park, and J.-H. Kim, "Hysteresis behavior of concrete filled square steel tube column-to-beam partially restrained composite connections", *J. Constr. Steel Res.* **66**:7 (2010), 943–953.

[Qin et al. 2014a] Y. Qin, Z. Chen, and B. Rong, "Component-based mechanical models for axially-loaded through-diaphragm connections to concrete-filled RHS columns", *J. Constr. Steel Res.* **102** (2014), 150–163.

[Qin et al. 2014b] Y. Qin, Z. Chen, Q. Yang, and K. Shang, "Experimental seismic behavior of through-diaphragm connections to concrete-filled rectangular steel tubular columns", *J. Constr. Steel Res.* **93**:1 (2014), 32–43.

[Rong et al. 2012] B. Rong, Z. Chen, R. Zhang, A. Fafitis, and N. Yang, "Experimental and analytical investigation of the behavior of diaphragm-through joints of concrete-filled tubular columns", *J. Mech. Mater. Struct.* **7**:10 (2012), 909–929.

[Rong et al. 2016] B. Rong, R. Liu, R. Zhang, Z. Chen, and A. Fafitis, "Flexural bearing capacity of diaphragm-through joints of concrete-filled square steel tubular columns", *Steel Compos. Struct.* **20**:3 (2016), 487–500.

[Tizani et al. 2013] W. Tizani, Z. Y. Wang, and I. Hajirasouliha, "Hysteretic performance of a new blind bolted connection to concrete filled columns under cyclic loading: an experimental investigation", *Eng. Struct.* **46** (2013), 535–546.

[Yin et al. 2016] L. Yin, G. Tang, M. Zhang, B. Wang, and B. Feng, "Monotonic and cyclic response of speed-lock connections with bolts in storage racks", *Eng. Struct.* **116** (2016), 40–55.

[Yu et al. 2015] Y. Yu, Z. Chen, and X. Wang, "Effect of column flange flexibility on WF-beam to rectangular CFT column connections", *J. Constr. Steel Res.* **106** (2015), 184–197.

Received 17 Mar 2017. Revised 7 Jul 2017. Accepted 8 Aug 2017.

BIN RONG: tjerobin@126.com
Tianjin University, Tianjin, China

CHANGXI FENG: fengchangxi95@163.com
Tianjin University, Tianjin, China

RUOYU ZHANG: zryu@163.com
Tianjin University, Tianjin, China

SHUAI LIU: lao_xs@163.com
Tianjin University, Tianjin, China

GUANGCHAO YOU: youguangchao@163.com
Tianjin University, Tianjin, China